AGU PUBLICATIONS

Geophysical Research Letters

RESEARCH LETTER
10.1002/2014GL061880

Key Points:
- Antarctic Circumpolar Current velocity was measured at Macquarie Ridge
- The current becomes more barotropic as it crosses the ridge
- Local nonlinear processes accelerate deep jet

Supporting Information:
- Readme
- Text S1
- Figure S1
- Figure S2
- Figure S3
- Figure S4

Correspondence to:
S. R. Rintoul,
Steve.Rintoul@csiro.au

Citation:
Rintoul, S. R., S. Sokolov, M. J. M. Williams, B. Peña Molino, M. Rosenberg, and N. L. Bindoff (2014), Antarctic Circumpolar Current transport and barotropic transition at Macquarie Ridge, *Geophys. Res. Lett.*, *41*, 7254–7261, doi:10.1002/2014GL061880.

Received 16 SEP 2014
Accepted 2 OCT 2014
Accepted article online 7 OCT 2014
Published online 23 OCT 2014

Antarctic Circumpolar Current transport and barotropic transition at Macquarie Ridge

S. R. Rintoul[1,2,3], S. Sokolov[1,2,3], M. J. M. Williams[4], B. Peña Molino[3], M. Rosenberg[3], and N. L. Bindoff[1,2,3,5,6]

[1]Oceans and Atmosphere Flagship, CSIRO, Hobart, Tasmania, Australia, [2]Centre for Australian Weather and Climate Research, Hobart, Tasmania, Australia, [3]Antarctic Climate and Ecosystems Cooperative Research Centre, University of Tasmania, Hobart, Tasmania, Australia, [4]National Institute of Water and Atmospheric Research, Wellington, New Zealand, [5]ARC Centre of Excellence in Climate System Science, Hobart, Tasmania, Australia, [6]Institute for Marine and Antarctic Studies, University of Tasmania, Hobart, Tasmania, Australia

Abstract Theory and numerical simulations suggest that topographic interactions are central to the dynamics of the Antarctic Circumpolar Current (ACC), but few observations are available to test these ideas. We use direct velocity measurements, satellite altimetry, and an ocean state estimate to investigate the interaction of the ACC with the Macquarie Ridge. Satellite altimeter data show that the Subantarctic Front crosses the ridge through a gap immediately north of Macquarie Island. Yearlong current meter records reveal strong deep mean flow ($> 0.2\,m\,s^{-1}$ at 3000 m) and substantial transport ($52 \pm 8 \times 10^6\,m^3\,s^{-1}$) in the 50 km wide gap. The ACC becomes much more barotropic at the ridge. Acceleration of the deep jet is balanced by the ageostrophic along-gap pressure gradient, convergence of zonal momentum by the mean vertical velocity, and dissipation. The study helps explain how the ACC negotiates large topographic obstacles and highlights the role of local, nonlinear processes in the dynamical balance of the ACC.

1. Introduction

The Antarctic Circumpolar Current (ACC) is the largest current in the world ocean, transporting 137–162 sverdrup (Sv; $1\,Sv = 10^6\,m^3\,s^{-1}$) from west to east along a 20,000 km path circling Antarctica [*Rintoul and Sokolov*, 2001; *Cunningham et al.*, 2003; *Legeais et al.*, 2005; *Meredith et al.*, 2011]. This interbasin connection allows the existence of a global-scale overturning circulation that largely determines the capacity of the ocean to store heat and carbon and thereby influence climate. The ACC also links the deep and upper limbs of the overturning circulation. Density surfaces shoal from north to south, in balance with the strong geostrophic flow of the ACC, and water mass transformations transfer water between density layers where these dense layers outcrop at the sea surface [*Speer et al.*, 2000; *Marshall and Speer*, 2012].

The absence of land barriers in the latitude band of Drake Passage means that a different dynamical balance applies than in midlatitude gyres [*Munk and Palmén*, 1951]. Wind and buoyancy forcing, eddy fluxes, and topographic interactions are central to the dynamics of the ACC [*Rintoul et al.*, 2001; *Olbers et al.*, 2004; *Hughes*, 2005; *Rintoul and Naveira Garabato*, 2013]. Momentum supplied by wind forcing is transferred vertically by interfacial form stress accomplished by standing and transient eddies; the wind stress is balanced by bottom form stress established by the interaction of deep flows with topographic features. Topographic interactions are also central to the barotropic vorticity budget of the ACC, where the dominant local balance is between advection of total vorticity and the bottom pressure torque resulting from deep flow crossing isobaths [*Hughes*, 2005]. The spatial distribution of mixing, eddy fluxes, and cross-front exchange is also influenced by topography [e.g., *Thompson*, 2010; *Thompson et al.*, 2010; *Naveira Garabato et al.*, 2012]. While theory and models suggest that interaction of the ACC with topography dominates the dynamical balance of the current, few observations have been available to test this hypothesis.

The Macquarie Ridge provides a major obstacle for the ACC, rising from depths of 5000 m to an average depth of 1500 m along the ridge crest between 47°S and 56°S. A large fraction of the current passes through a few narrow gaps in the ridge [*Gordon*, 1972]. These gaps provide a natural gate where the transport of ACC jets can be measured using a modest number of instruments. We use a spatially coherent array of near-full-depth velocity measurements in the gaps to determine the absolute transport and vertical shear of the Subantarctic Front where it crosses the Macquarie Ridge. We find that the flow becomes much more

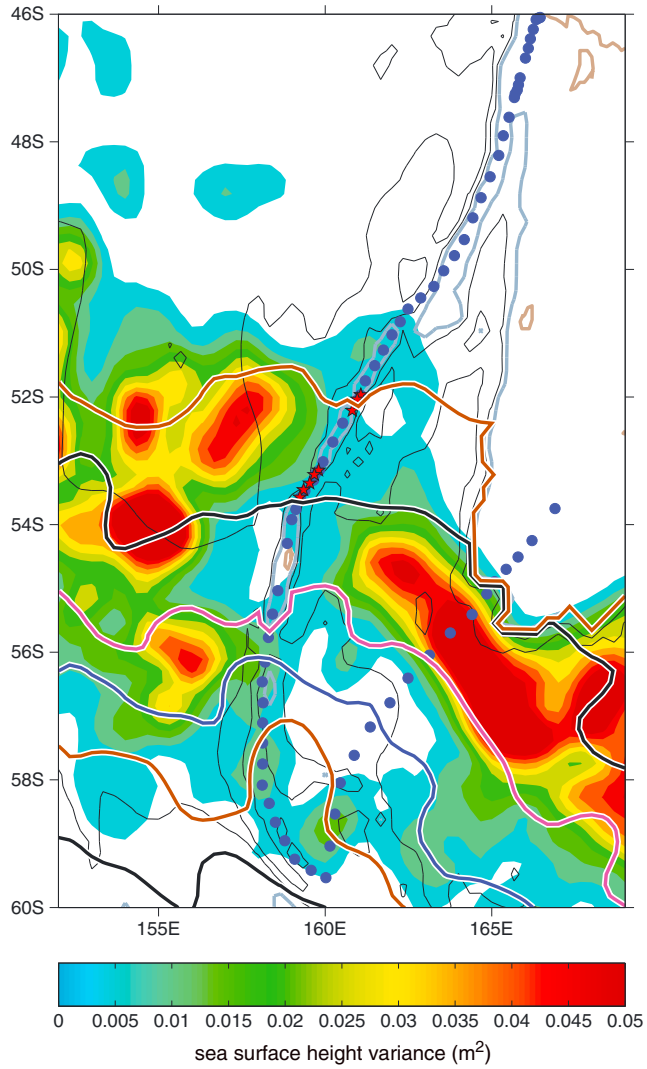

Figure 1. Location of moorings (red stars) and CTD measurements (blue dots and red stars) along the Macquarie Ridge in 2007. Sea surface height variance (m^2), calculated from satellite altimetry data between 1992 and 2011, is shown as a proxy for eddy kinetic energy (values less than 0.005 m^2 are blanked out). Mean positions of the fronts of the ACC during the period of the mooring observations are plotted as solid colored lines (from north to south: SAF-N, SAF-M, and SAF-S (brown, black, and magenta); PF-N, PF-M, and PF-S (blue, brown, and black); southern ACC front (magenta)). Bathymetry contours shown: coastline (thick light brown line), 2500 m isobath (thick grey line), and 3500 and 4300 m isobaths (thin grey lines).

barotropic where it crosses the ridge. The local dynamics of this barotropic transition are then explored using the Southern Ocean State Estimate (SOSE) [*Mazloff et al.*, 2010].

2. Data and Methods

Nine moorings were deployed for 12 months in two gaps in the ridge at 52.1°S and 53.3°S by R/V *Tangaroa* (Figure 1). One mooring in the northern gap was not recovered. A total of 35 current meters (Aanderaa Recording Current Meter (RCM)-7, RCM-8, and RCM-9), 34 conductivity-temperature (CT) recorders (Sea-Bird SBE 37), and two thermistors (Sea-Bird SBE 39) were recovered. Valid data were recorded by 67 of 71 instruments. Full-depth profiles of temperature and salinity were collected with a Sea-Bird SBE 911plus conductivity-temperature-depth (CTD) profiler along the crest of the ridge between New Zealand and 59.5°S during the deployment voyage in March 2007 (TAN0704) and the recovery voyage in April 2008 (TAN0803) (Figure 1). Full-depth temperature and salinity profiles were also obtained downstream of Macquarie Ridge during the deployment voyage in March 2007.

To calculate transport, 2-hourly measurements of velocity perpendicular to the direction of the ridge were linearly interpolated in 10 m vertical bins between depths of the uppermost and the deepest current meters on each mooring. The time-varying depth of each instrument, as measured by pressure sensors on the current meters, was used in the interpolation. Velocity at each 10 m bin was interpolated horizontally onto a 10 km grid using a smoothing spline. Mooring data were filtered to remove tides and other high-frequency signals using a low-pass filter with a cutoff frequency corresponding to a period of 1.5 days. Tilt of the moorings during strong current events was modest (e.g., exceeding 10° only 2.3% of the record for the top instrument at the mooring in the strong core of the SAF) and did not affect the operation of the gimbaled current meters. For transport calculations, velocity data were extrapolated to the sea surface and the seafloor using several methods: zero vertical shear, thin-plate spline, and constant vertical shear. The transport estimates reported here assume zero vertical shear above (below) the shallowest (deepest) current meter measurement (Figure S1 in the supporting information shows that the transport estimates are relatively insensitive to the choice of extrapolation method and that the zero shear assumption is conservative in that it results in lower transports than an assumption of constant shear).

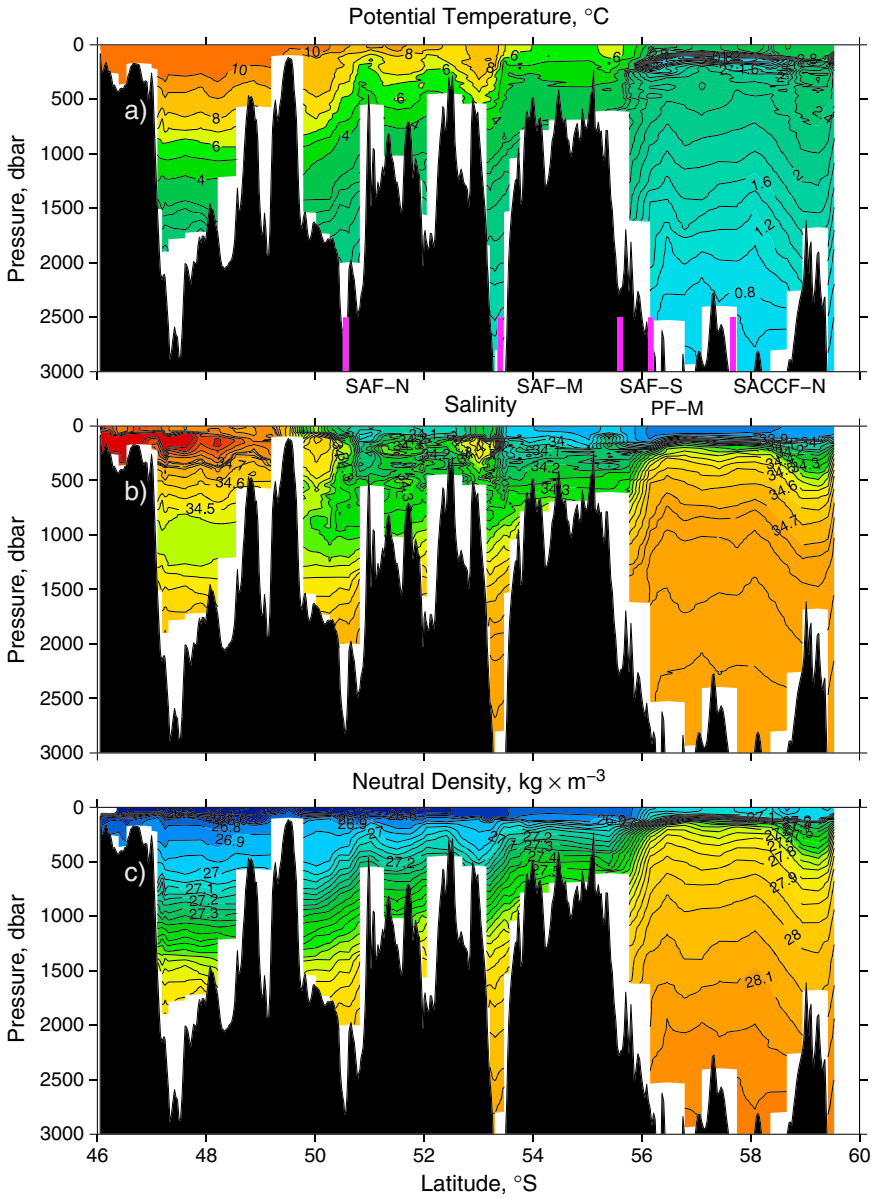

Figure 2. (a) Potential temperature, (b) salinity, and (c) neutral density in kg m^{-3} along the Macquarie Ridge in March 2007, during the deployment voyage. Magenta lines in Figure 2a indicate the mean position of the ACC fronts at the time of the voyage, inferred from temperature and salinity characteristics using the criteria in *Sokolov and Rintoul* [2007].

Satellite altimetry data were used to provide a broader spatial and temporal context for the measurements made over the ridge. The location of the ACC fronts (shown in Figure 1) was inferred from satellite altimetry data using the absolute sea surface height (SSH) values associated with each frontal branch [*Sokolov and Rintoul*, 2007, 2009].

The Southern Ocean State Estimate (SOSE) [*Mazloff et al.*, 2010] was used to diagnose the three-dimensional circulation and momentum budget in the vicinity of the ridge. SOSE is an eddy-permitting (1/6° horizontal resolution) ocean state estimate that assimilates a wide variety of observations in a dynamically consistent manner. The model has 42 vertical levels, with partial cells used to better represent sloping topography. The relatively high resolution, dynamical fidelity, and consistency with observations [*Mazloff et al.*, 2010; *Cerovečki et al.*, 2011; *Firing et al.*, 2011] of the model make SOSE a useful tool for investigating interactions between the ACC and topography. The transport through Drake Passage in SOSE is 153 ± 5 Sv, close to observed values. The total transport through the 53.3°S gap, integrated between the minima in surface velocity at

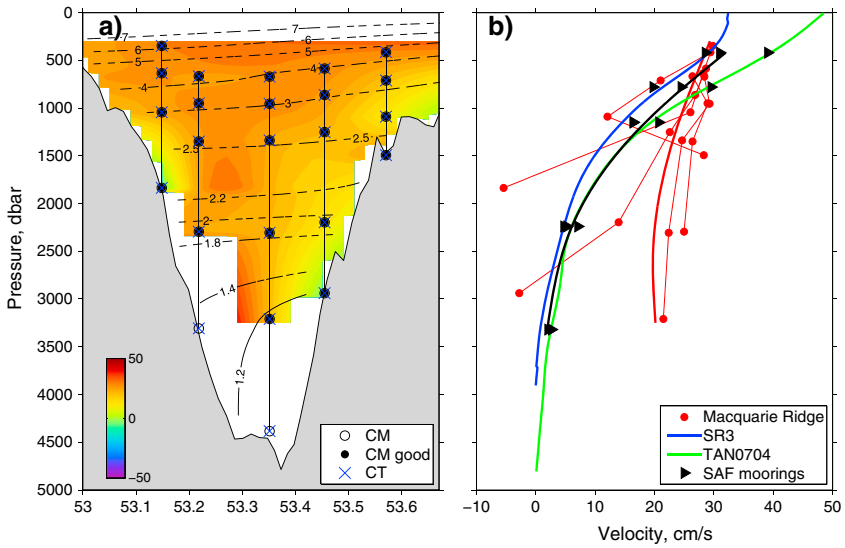

Figure 3. Flow through the 53.3°S gap in the Macquarie Ridge. (a) Mean through-passage speed measured by the current meter (CM) array. Positions of temperature and pressure sensors (CT) are also shown (open symbols indicate failed instruments). (b) Mean velocity profiles within the SAF: upstream, downstream, and in the southern gap of the Macquarie Ridge. Red dots indicate 1 year mean velocities from individual current meters shown in Figure 3a; red line is the area-weighted mean profile of through-passage speed. Black triangles indicate 2 year mean direct velocity measurements near 140°E, upstream of the ridge; black line is the mean profile from the current meters[14]. Blue line is geostrophic velocity calculated from hydrographic data at 140°E; green line is geostrophic velocity calculated from hydrographic data from the R/V *Tangaroa* section downstream of the ridge (see Figure 1).

either side of the gap (Figure S3), is 50 ± 9 Sv in SOSE, in agreement with the 52 ± 8 Sv estimated from the mooring data. However, both the bathymetry and the fronts are smoother in the model than observed (compare Figures 2 and 3 to Figures S2 and S3). When integrated over the latitude band spanned by the moored array in the 53.3°S gap, SOSE has a transport of 30 ± 9 Sv.

3. Results

Potential temperature, salinity, and density sections illustrate the multiple filaments of the ACC and their interaction with the ridge (Figure 2). The largest horizontal gradients (and hence strongest velocities) are located in gaps in the ridge to the north and south of Macquarie Island. The enhanced horizontal gradients extend throughout the water column, reflecting the deep-reaching nature of the ACC jets. The temperature and salinity characteristics [*Sokolov and Rintoul*, 2007] identify the jets as the northern branch of the Subantarctic Front (SAF-N) at 50.5°S and 52.1°S, the middle branch of the Subantarctic Front (SAF-M) at 53.3°S, and a combined SAF-S and northern Polar Front (PF-N) immediately to the south of Macquarie Island. The distribution of potential temperature and transport along the ridge crest in SOSE is similar to the observations (Figure S3), with the largest surface speed and transport found where the SAF flows through the gap in the ridge at 53.3°S.

Each of the ACC jets tends to be associated with a particular sea surface height (SSH) contour [*Sokolov and Rintoul*, 2007, 2009]. The position of the jets can therefore be inferred from weekly maps of SSH derived from satellite altimetry. During the period of the mooring observations, the core of the SAF (SAF-M) passed through the moored array in the 53.3°S gap 96% of the time (Figure 1 and Table S1). The northern branch of the SAF is more variable, passing through the instrumented gap at 52.1°S 76% of the time, through a gap at 50.5°S 20% of the time, and through the 53.3°S gap 3% of the time. The full 18 year (1992 to 2011) altimeter record shows a similar pattern (Table S1). Mean kinetic energy exceeds eddy kinetic energy at individual current meters by a factor between 3 and 17 (not shown), reflecting the steadiness of the flow through the 53.3°S gap. Sea surface height variability (a proxy for eddy kinetic energy) is high up and downstream of the ridge but low over the ridge itself (Figure 1).

The mean velocity at the 53.3°S gap is strongly eastward, with speeds greater than 0.2 m s^{-1} from 500 m to >3000 m depth in the middle of the passage (Figure 3). The flow through the gap is much more barotropic

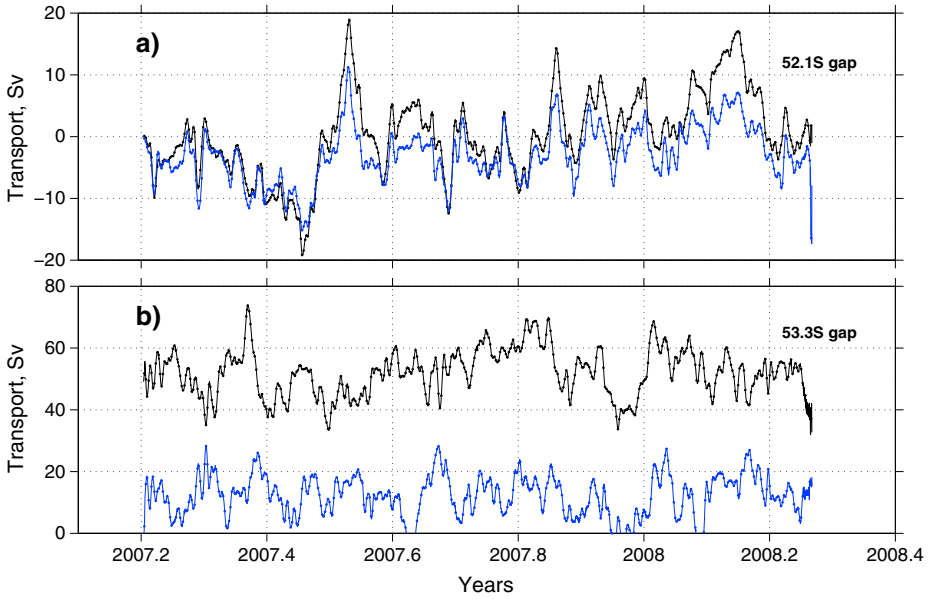

Figure 4. Total (black) and baroclinic (blue) transport through the gaps in the ridge at (top) 52.1°S and (bottom) 53.3°S. The baroclinic transport is calculated by subtracting the velocity measured at the deepest current meter on each mooring from the total velocity.

than observed at locations distant from the ridge. The vertical shear of the SAF between 500 and 3500 m is 4 times smaller in the gap than observed upstream at 140°E [*Phillips and Rintoul*, 2000], downstream south of the Campbell Plateau (Figure 3b), and in mooring data adjacent to the Campbell Plateau [*Stanton and Morris*, 2004]. (Vertical and horizontal shears are larger near the flanks of the gap, where dissipation likely plays a greater role, in both the observations (Figure 3) and the model (Figure S1)).

The net transport through the 53.3°S gaps is 52 ± 8 Sv (Figure 4; see section 2 and Figure S1 for integration approach; error is 1 standard deviation). The 95% confidence intervals on the mean are narrow (±1.7 Sv, with a decorrelation time scale of 10.5 days), and the cumulative average of the transport lies within this confidence interval within 6 months, indicating that the current meter records are of sufficient duration to establish a stable mean. As anticipated from Figure 3, the transport is strongly barotropic, with 80% of the net flow carried by the depth-independent component, compared to 14% in the barotropic mode at 140°E [*Phillips and Rintoul*, 2002] (the barotropic transport is estimated in each case by multiplying the deepest available current meter measurements by the water depth).

The flow through the shallower gap at 52.1°S is weaker, more baroclinic, and oscillates in sign, with little net transport (0.3 ± 7 Sv) (Figures 4, S2, and S4). However, the failure to recover one mooring from the northern array makes the transport estimates less certain there. SSH data (not shown) confirm that the branch of the SAF passing through the northern gap is more variable and occasionally flows from east to west, consistent with Figure 4. The shallow depth of the northern gap may divert part of the jet (e.g., to the deeper, uninstrumented gap at 50.5°S), resulting in weaker and more baroclinic flow than observed in the deeper gap at 53.3°S.

The transition to barotropic flow in the 53.3°S gap is also seen in the SOSE model (Figure S3). The model fields can be used to examine the dynamics responsible for the acceleration of the deep flow. The time-mean zonal momentum budget is

$$\frac{\partial \overline{u}^2}{\partial x} = -\frac{\partial \overline{v}\,\overline{u}}{\partial y} - \frac{\partial \overline{w}\,\overline{u}}{\partial z} - \frac{\partial \overline{u'^2}}{\partial x} - \frac{\partial \overline{v'u'}}{\partial y} - \frac{\partial \overline{w'u'}}{\partial z} - \frac{\partial p}{\partial x} + f\overline{v} + F_x$$

where u, v, and w are the zonal, meridional, and vertical components of the velocity, f is the Coriolis acceleration, p is the pressure, and F_x represents the frictional terms. Overbars denote time averages, and primes denote departures from the time mean. The intensification of the eastward mean flow (term on left-hand side) is balanced by the meridional and vertical divergence of momentum flux by the mean flow (terms 2 and 3),

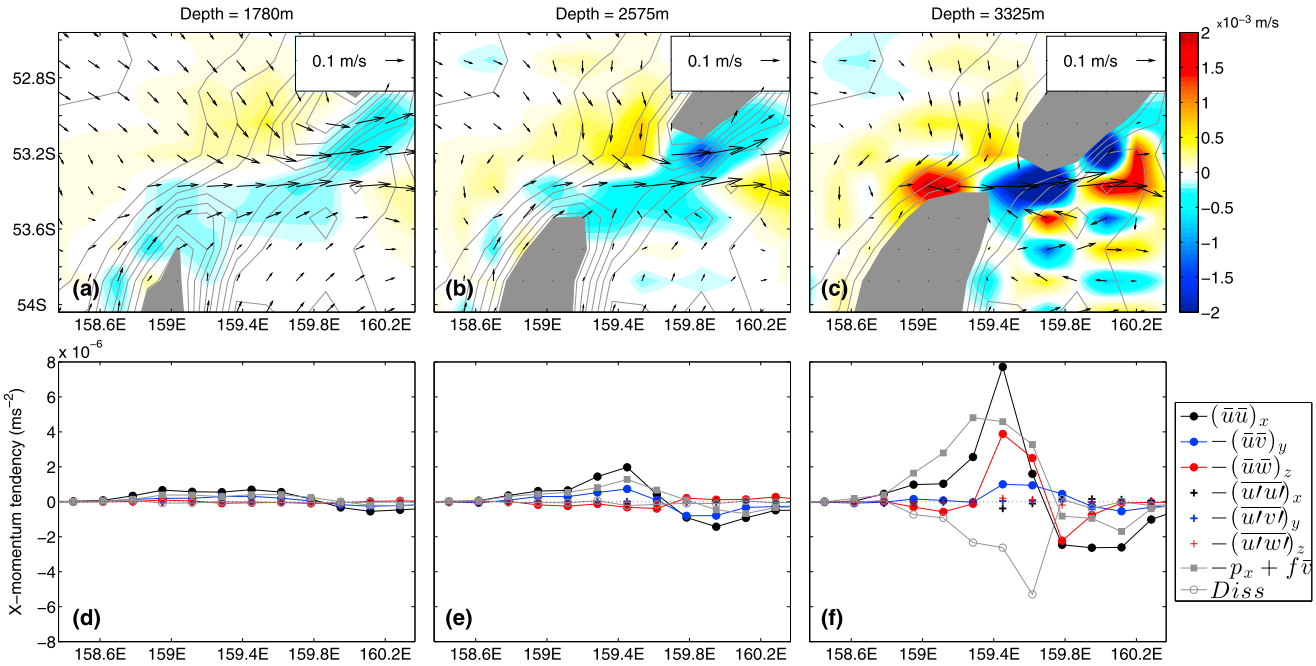

Figure 5. (a–c) Mean horizontal (vectors) and vertical velocity (color) at three depths in the vicinity of the Macquarie Ridge, from SOSE. Positive vertical velocity is upward (red shades). The model bathymetry is shown by the grey contours. (d–f) Terms in the mean zonal momentum budget at a constant latitude passing through the center of the gap (approximately 53.3°S), at the same three depths. See text for explanation of the symbols used in the legend in Figures 5d–5f. Positive values indicate acceleration of the flow. The momentum dissipation (Diss) is the sum of biharmonic and Laplacian friction in the horizontal and Laplacian friction in the vertical. The dissipation terms were only archived in the 30 day average fields. As the eddy terms are weak, the terms in the momentum budget calculated from 5 day average fields are indistinguishable from those computed using 30 day averages (Figure 5f).

the zonal, meridional, and vertical divergence of momentum flux due to eddies (terms 4–6), the zonal pressure gradient (term 7), the Coriolis force (term 8), and friction. The contribution from each of the terms is illustrated in Figure 5 for three depths below the crest of the ridge. Since the flow is largely in geostrophic balance, the pressure gradient term and Coriolis force have been combined into a single term, which represents the along-gap pressure gradient that is not in geostrophic balance. The contribution from eddies is negligible. At each depth, the zonal flow accelerates upstream and through the gap and decelerates downstream of the gap, within 35 km of the ridge crest. At depths where the gap is sufficiently broad (2500 m and above), the intensification and weakening of the zonal flow are due to the meridional momentum flux by the mean flow and the ageostrophic pressure gradient. Deeper in the water column, where more latitudes become blocked by the ridge, flux of eastward momentum by the mean vertical velocity contributes to the acceleration of the zonal flow. At the deepest level dissipation becomes important in the immediate vicinity of the gap (Figure 5f).

The mean vertical velocity (~2×10^{-3} m s^{-1}) at the gap is large relative to values typical of the ACC in deep water (e.g., 0.01–0.2×10^{-3} m s^{-1} at 140°E [*Phillips and Rintoul*, 2000]). Large vertical velocities at the bottom equate to large bottom pressure torques ($fw_b = \nabla P \cdot \nabla h$, where w_b is the vertical velocity at the bottom, P is bottom pressure, and h is water depth [*Hughes and de Cuevas*, 2001; *Hughes*, 2005]).

4. Discussion

Most previous estimates of the transport of ACC fronts have relied on snapshots from ship-based instrumentation or incoherent moored arrays; strong meandering of the ACC jets further complicates attempts to measure transport with a small number of moorings in fixed locations. The geometry of the Macquarie Ridge constrains the main branch of the SAF to pass through the 53.3°S gap, allowing accurate and stable estimates of transport. We find that $52 \pm 8 \times 10^6$ m^3 s^{-1}, about 30% of the total transport of the ACC, passes through a single gap in the Macquarie Ridge with a mean width of 50 km. As transport of the ACC is a common metric used to assess the realism of numerical simulations, these results provide a useful target for ocean models.

The SAF transitions from baroclinic to barotropic flow over the ridge. Strong ($>0.10\,m\,s^{-1}$) near-bottom velocities have also been observed where the SAF [*Smith et al*., 2010] and Polar Front [*Walkden et al*., 2008; *Damerell et al*., 2012] cross the North Scotia Ridge, in Drake Passage [*Chereskin et al*., 2009], and where the Southern ACC Front crosses the Kerguelen Plateau through Fawn Trough [*Sekma et al*., 2013]. Previous studies have not, however, explored the dynamics of the barotropic transition over topography. We find that the ageostrophic along-gap pressure gradient and vertical convergence of eastward momentum by the mean flow are responsible for accelerating and decelerating the deep jet in the ridge gap in the SOSE model. While the importance of topographic interactions in the momentum and vorticity budgets of the ACC jets has long been recognized [e.g., *Munk and Palmén*, 1951], the dynamics responsible have remained obscure. The insights gained here from observations and a dynamically realistic ocean state estimate help explain how the ACC negotiates large topographic obstacles.

The deep flow through the gap is remarkably steady, with mean kinetic energy exceeding eddy kinetic energy by more than an order of magnitude below 2000 m depth, and eddy fluxes play a small role in the barotropic transition over the ridge in SOSE. This result is in contrast to the ACC as a whole, for which an abundant literature documents the importance of eddies in the dynamics of the ACC (see reviews by *Rintoul et al*. [2001], *Olbers et al*. [2004], and *Marshall and Speer* [2012, and references therein]). In particular, eddy kinetic energy is often enhanced in the lee of topographic obstacles [*Fu*, 2009; *Lu and Speer*, 2010; *Sallée et al*., 2011], where eddy fluxes make a significant contribution to the momentum and vorticity budgets of the ACC and to transport across fronts [e.g., *Williams et al*., 2007; *Naveira Garabato et al*., 2011; *Thompson and Sallée*, 2012; *Thompson and Naveira Garabato*, 2014]. Eddy vorticity forcing may help steer the ACC through gaps in topography [*Williams et al*., 2007]. At the ridge itself, however, the flow is strongly constrained by topography, eddy forcing is weak, and momentum convergence by the mean flow helps to accelerate the deep jet. The results highlight the distinct dynamics of the flow through the ridge gap and underscore the importance of local processes in the dynamical balance and circulation of the ACC.

Acknowledgments

We thank the Captain and crew of R/V *Tangaroa* for their assistance in deploying and recovering the moorings and Matthew Mazloff for providing the SOSE output. We thank Chris Hughes and an anonymous reviewer for their useful comments and suggestions. The work was supported in part by the Cooperative Research Centre program of the Australian Government, through the Antarctic Climate and Ecosystems Cooperative Research Centre; by the Australian Government Department of the Environment, the Bureau of Meteorology and CSIRO through the Australian Climate Change Science Program; and by NIWA through core funding under the National Climate Centre Research Climate Observations program. N.L.B. acknowledges support from the ARC Centre of Excellence for Climate System Science (CE110001028). The data are available from the Antarctic Climate and Ecosystems Cooperative Centre (mark.rosenberg@utas.edu.au).

Meghan Cronin thanks Christopher Hughes and one anonymous reviewer for their assistance in evaluating this paper.

References

Cerovečki, I., L. D. Talley, and M. R. Mazloff (2011), A comparison of Southern Ocean air-sea buoyancy flux from an ocean state estimate with five other products, *J. Clim.*, *24*(24), 6283–6306, doi:10.1175/2011JCLI3858.1.

Chereskin, T. K., K. A. Donohue, D. R. Watts, K. L. Tracey, Y. L. Firing, and A. L. Cutting (2009), Strong bottom currents and cyclogenesis in Drake Passage, *Geophys. Res. Lett.*, *36*, L23602, doi:10.1029/2009GL040940.

Cunningham, S. A., S. G. Alderson, B. A. King, and M. A. Brandon (2003), Transport and variability of the Antarctic Circumpolar Current in Drake Passage, *J. Geophys. Res.*, *108*, 8084, doi:10.1029/2001JC001147.

Damerell, G. M., K. J. Heywood, D. P. Stevens, and A. C. Naveira Garabato (2012), Temporal variability of diapycnal mixing in Shag Rocks Passage, *J. Phys. Oceanogr.*, *42*, 370–385.

Firing, Y. L., T. K. Chereskin, and M. R. Mazloff (2011), Vertical structure and transport of the Antarctic Circumpolar Current in Drake Passage from direct velocity observations, *J. Geophys. Res.*, *116*, C08015, doi:10.1029/2011JC006999.

Fu, L. (2009), Pattern and velocity of propagation of the global ocean eddy variability, *J. Geophys. Res.*, *114*, C11017, doi:10.1029/2009JC005349.

Gordon, A. L. (1972), On the interaction of the Antarctic Circumpolar Current and the Macquarie Ridge, in *Antarctic Oceanology II: The Australian-New Zealand Sector*, *Antarctic Res. Ser.*, vol. 19, edited by D. E. Hayes, pp. 71–78, AGU, Washington, D. C.

Hughes, C. W. (2005), Nonlinear vorticity balance of the Antarctic Circumpolar Current, *J. Geophys. Res.*, *110*, C11008, doi:10.1029/2004JC002753.

Hughes, C. W., and B. A. de Cuevas (2001), Why western boundary currents in realistic oceans are inviscid: A link between form stress and bottom pressure torque, *J. Phys. Oceanogr.*, *31*, 2871–2885.

Legeais, J. F., S. Speich, M. Arhan, I. Ansorge, E. Fahrbach, S. Garzoli, and A. Klepikov (2005), The baroclinic transport of the Antarctic Circumpolar Current south of Africa, *Geophys. Res. Lett.*, *32*, L24602, doi:10.1029/2005GL023271.

Lu, J., and K. Speer (2010), Topography, jets, and eddy mixing in the Southern Ocean, *J. Mar. Res.*, *68*, 479–502.

Marshall, J., and K. Speer (2012), Closure of the meridional overturning circulation through Southern Ocean upwelling, *Nat. Geosci.*, *5*, 171–180, doi:10.1038/NGEO1391.

Mazloff, M. R., P. Heimbach, and C. Wunsch (2010), An eddy-permitting Southern Ocean State Estimate, *J. Phys. Oceanogr.*, *40*, 880–899.

Meredith, M. P., et al. (2011), Sustained monitoring of the Southern Ocean at Drake Passage: Past achievements and future priorities, *Rev. Geophys.*, *49*, doi:10.1029/2010RG000348.

Munk, W. H., and E. Palmén (1951), Note on the dynamics of the Antarctic Circumpolar Current, *Tellus*, *3*, 53–55.

Naveira Garabato, A. C., R. Ferrari, and K. L. Polzin (2011), Eddy stirring in the Southern Ocean, *J. Geophys. Res.*, *116*, C09019, doi:10.1029/2010JC006818.

Naveira Garabato, A. C., A. J. Nurser, S. George, B. Robert, and J. A. Goff (2013), The impact of small-scale topography on the dynamical balance of the ocean, *J. Phys. Oceanogr.*, *43*(3), 647–668, doi:10.1175/JPO-D-12-056.1.

Olbers, D., D. Borowski, C. Volker, and J.-O. Wolff (2004), The dynamical balance, transport and circulation of the Antarctic Circumpolar Current, *Antarct. Sci.*, *16*, 439–470, doi:10.1017/S0954102004002251.

Phillips, H. E., and S. R. Rintoul (2000), Eddy variability and energetics from direct current measurements in the Antarctic Circumpolar Current south of Australia, *J. Phys. Oceanogr.*, *30*, 3050–3076.

Phillips, H. E., and S. R. Rintoul (2002), A mean synoptic view of the Subantarctic Front south of Australia, *J. Phys. Oceanogr.*, *32*, 1536–1553.

Rintoul, S. R., and A. C. Naveira Garabato (2013), Chapter 18: Dynamics of the Southern Ocean Circulation, in *Ocean Circulation and Climate, 2nd Ed. A 21st Century Perspective*, *Int. Geophys. Ser.*, vol. 103, edited by G. Siedler et al., Academic Press, Oxford, U. K.

Rintoul, S. R., and S. Sokolov (2001), Baroclinic transport variability of the Antarctic Circumpolar Current south of Australia (WOCE repeat section SR3), *J. Geophys. Res.*, *106*, 2795–2814, doi:10.1029/2000JC900117.

Rintoul, S. R., C. Hughes, and D. Olbers (2001), The Antarctic Circumpolar Current system, in *Ocean Circulation and Climate*, edited by G. Siedler, J. A. Church, and J. Gould, pp. 271–302, Academic Press, New York.

Sallée, J.-B., K. Speer, and S. R. Rintoul (2011), Mean-flow and topographic control on surface eddy-mixing in the Southern Ocean, *J. Mar. Res.*, *69*, 753–777.

Sekma, H., Y.-H. Park, and F. Vivier (2013), Time-mean flow as the prevailing contribution to the poleward heat flux across the southern flank of the Antarctic Circumpolar Current: A case study in the Fawn Trough, Kerguelen Plateau, *J. Phys. Oceanogr.*, *43*, 583–601.

Smith, I. J., D. P. Stevens, K. J. Heywood, and M. P. Meredith (2010), The flow of the Antarctic Circumpolar Current over the North Scotia Ridge, *Deep Sea Res., Part I*, *57*, 14–28.

Sokolov, S., and S. R. Rintoul (2007), Multiple jets of the Antarctic Circumpolar Current south of Australia, *J. Phys. Oceanogr.*, *37*, 1394–1412.

Sokolov, S., and S. R. Rintoul (2009), Circumpolar structure and distribution of the Antarctic Circumpolar Current fronts: 1. Mean circumpolar paths, *J. Geophys. Res.*, *114*, C11018, doi:10.1029/2008JC005108.

Speer, K., S. R. Rintoul, and B. Sloyan (2000), The diabatic Deacon cell, *J. Phys. Oceanogr.*, *30*, 3212–3222.

Stanton, B. R., and M. Y. Morris (2004), Direct velocity measurements in the Subantarctic Front and over Campbell Plateau, southeast of New Zealand, *J. Geophys. Res.*, *109*, C01028, doi:10.1029/2002JC001339.

Thompson, A. F. (2010), Jet formation and evolution in baroclinic turbulence with simple topography, *J. Phys. Oceanog.*, *40*, 257–278, doi:10.1175/2009JPO4218.1.

Thompson, A. F., and A. C. Naveira Garabato (2014), Equilibration of the Antarctic Circumpolar Current by standing meanders, *J. Phys. Oceanogr.*, *44*, 1811–1828.

Thompson, A. F., and J.-B. Sallée (2012), Jets and topography: Jet transitions and impacts on transport, *J. Phys. Oceanogr.*, *42*, 956–972.

Thompson, A. F., P. H. Haynes, C. Wilson, and K. J. Richards (2010), Rapid Southern Ocean front transitions in an eddy-resolving ocean GCM, *Geophys. Res. Lett.*, *37*, L23602, doi:10.1029/2010GL045386.

Walkden, G. J., K. J. Heywood, and D. P. Stevens (2008), Eddy heat fluxes from direct current measurements of the Antarctic Polar Front in Shag Rocks Passage, *Geophys. Res. Lett.*, *35*, L06602, doi:10.1029/2007GL032767.

Williams, R. G., C. Wilson, and C. W. Hughes (2007), Ocean and atmosphere storm tracks: The role of eddy vorticity forcing, *J. Phys. Oceanog.*, *37*, 2267–2289.